Available online at www.sciencedirect.com
ScienceDirect
Journal of the European Ceramic Society 28 (2008) 2225–2232
www.elsevier.com/locate/jeurceramsoc

# Sintering of thin film nanocrystalline titania–tin oxide composites

Johanna Wallot [a,*], Peter Reynders [b], Andrew A. Herzing [c], Christopher J. Kiely [c], Martin P. Harmer [c], Jürgen Rödel [a]

[a] *Technische Universität Darmstadt, Institute of Materials Science, Petersenstr. 23, Darmstadt D-64287, Germany*
[b] *Merck KGaA, Darmstadt D-64271, Germany*
[c] *Center for Advanced Materials and Nanotechnology, Lehigh University, 5 Packer Avenue, Bethlehem, PA 18015, USA*

Received 12 October 2007; received in revised form 12 February 2008; accepted 29 February 2008

**Abstract**

Thin nanocrystalline titania films were sintered on dense substrates with the addition of tin(IV) oxide as a possible grain growth inhibitor. Densification and the development of the pore size distribution were examined via nitrogen adsorption. Aberration-corrected scanning transmission electron microscopy (STEM) and X-ray energy dispersive spectroscopy (XEDS) studies combined with X-ray spectroscopy measurements were carried out to investigate the tin and titanium distribution in the thin films. These studies showed that the additions of $SnO_2$ have little influence on grain growth during sintering of nanocrystalline titania films, but can strongly affect the phase transition from anatase to rutile. The influence of this phase transition during sintering in thin films and the effect on the in-plane biaxial stresses is highlighted.


*Keywords:* Films; Sintering; Phase transformation; $TiO_2$; $SnO_2$

## 1. Introduction

Titania is a very important material for various purposes. Due to its whiteness it is a common additive in wall paints, paper production and sunscreens. Because it is semi-conductive, thin layers or coatings of $TiO_2$ are also used in solar cells, such as the so called Graetzel cell.[1,2] As a photocatalyst it is used on ceramic tiles or on glass[3] to produce a self-cleaning surface,[4,5] in addition to exhibiting an antifogging effect.[3,6]

For photocatalytic purposes such as self-cleaning windshields,[4,5] small particles are required to minimize scattering of light and to maintain transparency of the glass. Therefore, the particles must be much smaller than 400 nm, preferably around 3–5 nm in diameter.[4]

$TiO_2$ can exist in three crystalline modifications: brookite (orthorhombic), anatase (tetragonal) and rutile (tetragonal); however, rutile is the only thermodynamically stable form.[7] The anatase form is usually synthesized at low temperatures and transforms to rutile between 600 °C and 900 °C.[7–9]

Thin titania layers can be prepared in different ways. In this study a precipitation process was used to coat thin muscovite platelets with $TiO_2$. Under these conditions, the titania is sintered under geometrical constraint, and the transformation to rutile is hindered.[10,11] The formation of rutile via a low temperature processing route is only possible if the substrate is pre-coated with tin(IV) oxide.[7,12] Therefore, a thin $SnO_2$ layer is first precipitated on the substrate. During the subsequent precipitation of titania, rutile develops preferentially to anatase due to the commonality in crystal structure and similarity in lattice parameters between rutile and tin oxide.[7]

Nanocrystalline materials tend to sinter at lower sintering temperatures and show enhanced grain growth as compared to microcrystalline materials,[13–15] so it is often necessary to introduce a second phase to inhibit grain growth. For instance, Srdic et al. showed that the addition of a certain amount of nanocrystalline alumina yields a decrease in grain growth during the sintering of nanocrystalline zirconia.[16]

In the present case of nanocrystalline $TiO_2$, a small amount of nanocrystalline tin(IV) oxide was chosen as a second phase additive, since it is reported to form a miscibility gap with titania when sintered at or below 900 °C[17] and is compatible with the process for manufacturing thin titania films. Thus, $TiO_2$ films doped with three different amounts of tin(IV) oxide were co-

* Corresponding author. Tel.: +49 6151 166311; fax: +49 6151 166314.
*E-mail address:* wallot@ceramics.tu-darmstadt.de (J. Wallot).

0955-2219/$ – see front matter © 2008 Elsevier Ltd. All rights reserved.
doi:10.1016/j.jeurceramsoc.2008.02.019

precipitated on muscovite and the sintering behaviour compared to films of pure anatase and pure rutile. Scanning transmission electron microscopy (STEM) studies were also carried out to investigate the tin distribution in the co-precipitated and rutile thin films.

## 2. Experimental procedures

In order to obtain thin titania films, a 40 wt.% aqueous $TiOCl_2$ solution (Merck KGaA, Germany, Art. No. 2/78280) was added to an aqueous suspension containing 5 wt.% approximately 300 nm thick muscovite platelets and the pH adjusted to 2 using NaOH. During this process, a uniform thin layer of nanocrystalline anatase ($TiO_2$) precipitated on the platelets. Its thickness was adjusted to 60 nm by controlling the amount of $TiOCl_2$ solution added. The mean primary particle size after deposition was about 8 nm.[18]

For producing tin oxide-doped films three different amounts of $SnO_2$ (3.4 wt.%, 5.7 wt.% and 8.7 wt.%) relative to $TiO_2$, (hereafter referred to as T + S3.4, T + S5.7 and T + S8.7, respectively) were added during precipitation by using a $SnCl_4$ solution as a precursor. The same precipitation conditions as for the pure anatase films were used.

For comparative purposes pure rutile films were also produced.[19] The formation of rutile via a low temperature processing route is only possible if the substrate is pre-coated with tin(IV) oxide.[7,12] Therefore, a thin $SnO_2$ layer was first precipitated on the substrate by using a $SnCl_4$ solution. Afterwards $TiO_2$ was precipitated as described above.

A systematic series of films were subsequently sintered isothermally in a preheated furnace at 400 °C, 500 °C, 600 °C, 700 °C, 800 °C and 900 °C for 30 min each.

Nitrogen adsorption (Model No. Autosorb 3b, Quantachrome Corp., Boynton Beach, FL) was used to obtain the Brunauer–Emmett–Teller (BET) surface areas,[20–22] the relative densities of the thin films, and the pore size distributions within the thin films. Grain sizes were determined from topographic secondary electron images of the layers acquired using a high-resolution scanning electron microscope (SEM; Model No. XL 30 FEG, Philips Electronic Instruments, Mahwah, NJ).

Surface area data were obtained by placing samples of the thin films in a glass tube and tempering for 24 h at 250 °C. The amount of adsorbed nitrogen gas was measured with increasing and decreasing relative gas pressure. The full isotherm was obtained by taking 40 adsorption and 40 desorption data points. The specific surface area (BET) of the green and the sintered samples was characterised by utilizing the adsorption data in the relative pressure range of 0.05–0.3.[21]

According to the IUPAC classification,[22] all the isotherms of the films were of type IV. The adsorbed gas volume at a relative pressure of 0.98 could be used to calculate the total pore volume of the layers. The influence of the substrate was taken to be negligible for the calculation of the relative density of the film, and the weight fraction of $TiO_2$ was measured via X-ray fluorescence analysis (ARL ADVANT XP-518).

Commonly, data from the desorption branch are used to determine the pore size distribution,[23,24] but this is correct only if the hysteresis loop closes at a relative pressure of about 0.42. For cases, where the hysteresis loop does not close at this relative pressure, it is advisable to use the adsorption data to avoid computation with too large adsorbed gas volume.[22] The absence of the closure point of the hysteresis loop is often an effect of pore geometry since the gas cannot completely escape during the desorption process if the pore necks are too small.

Using the theory of Barrett et al.,[25] who assumed the validity of the Kelvin equation and a cylindrical pore geometry, the size distribution of meso-pores (2–50 nm in diameter) can be calculated.[23] Grain size was measured taking four high-resolution images for each specimen and using a line intercept method.[11] 50 intersections were needed on each picture.

Rutile (4.26 g/cm$^3$) and anatase (3.84 g/cm$^3$) have significantly different densities. Thus, Raman spectroscopy (Bruker RFS 100/S) was utilized to assess the relative contents of rutile and anatase in order to compute the theoretical densities of each specimen. These measurements were carried out on thin film specimens that were dried at 95 °C and subsequently sintered either at 600 °C or at 850 °C. To calculate the relative densities of specimens with the other sintering temperatures, we assumed that the rutile content increases linearly from 600 °C to 850 °C since it is reported that the $TiO_2$ polymorphic transformation takes place between 600 °C and 800 °C.[8]

The tin distribution was determined in co-precipitated films and at a sharp interface between tin oxide and rutile film. For the latter, 140 nm thick films of rutile were precipitated on corundum flakes since they are more stable up to higher sintering temperatures than muscovite platelets. At the interface a thin film of tin oxide had been pre-deposited. T + S8.7 films sintered at 900 °C and the rutile films sintered at 700 °C and 900 °C were then analyzed via X-ray energy dispersive spectroscopy (XEDS) using a Vacuum Generators HB 603 dedicated STEM operating at 300 kV and equipped with a nion spherical aberration corrector. This instrument is also equipped with an Oxford INCA 300 system for XEDS spectrum image acquisition in order to produce elemental maps of the samples. Therefore, small amounts of powders were mounted in epoxy-resin and dried overnight. In order to generate electron transparent specimens that were suitable for STEM–XEDS analysis, thin slices, 40–60 nm in thickness, were cut with a microtome from the dried resin and captured on a TEM copper grid. Each grid supported 4–8 of these samples.

## 3. Results

Table 1 summarizes the compositions and the rutile contents of the four different layers examined. The pure anatase film T and also the film T + S3.4 contain no rutile after drying and after sintering. If the tin(IV) oxide content rises, some rutile is obtained. In film T + S5.7 and T + S8.7, 10 wt.% rutile was detected after drying. After calcination at 850 °C, film T + S8.7 contains nearly 90 wt.% rutile.

Fig. 1(a) depicts the evolution of grain size as a function of sintering temperature for the different films. All of the films exhibited a starting grain size of approximately 8 nm. With increased sintering temperature, the grain size increases and

Table 1
Rutile contents of dried and calcined specimens undoped and doped with $SnO_2$

| Specimen | Rutile content (wt.%) after drying at 110 °C | Rutile content (wt.%) after sintering at 850 °C for 0.5 h |
|---|---|---|
| T ($TiO_2$ on muscovite) | 0 | 0 |
| T + S3.4 (3.4 wt.% $SnO_2$ with $TiO_2$ on muscovite) | 0 | 0 |
| T + S5.7 (5.7 wt.% $SnO_2$ with $TiO_2$ on muscovite) | ~10 | ~80 |
| T + S8.7 (8.7 wt.% $SnO_2$ with $TiO_2$ on muscovite) | ~10 | ~90 |

reaches an average value of about 60 nm after sintering at 900 °C. Considering the error bars, no significant differences between the average grain size of the different films can be discerned, and no effect of $SnO_2$ on grain growth is obtained. Fig. 1(b) shows the corresponding relative density versus sintering temperature for the same four samples. With increased sintering temperature, the relative density of all specimens increases, but to a lesser degree for samples with 5.7 wt.% and 8.7 wt.% tin(IV) oxide as compared to pure titania (anatase) films or with 3.4 wt.% $SnO_2$-doped films. While the pure titania film T reaches a relative density of about 73% at 900 °C, the films T + S5.7 and T + S8.7 only reach a relative density of about 64%, despite having almost identical starting densities. As shown in Table 1, if a small volume fraction of rutile phase exists after the drying step, the resulting density increase after sintering at high temperatures is smaller compared to that of a pure $TiO_2$ film.

The data in Fig. 1a and b can be combined to form the sintering trajectories for the films as shown in Fig. 2. Film T and T + S3.4 exhibit the expected usual sintering trajectories of nanocrystalline materials.[15] However, a large amount of tin(IV) oxide leads to a significantly decreased density as is the case for T + S5.7 and T + S8.7, which show considerable grain growth but poor densification.

The nitrogen adsorption isotherms of the non-sintered pure $TiO_2$ films are presented in Fig. 3 where the hysteresis loop does not close until a relative pressure of 0.05 is reached.

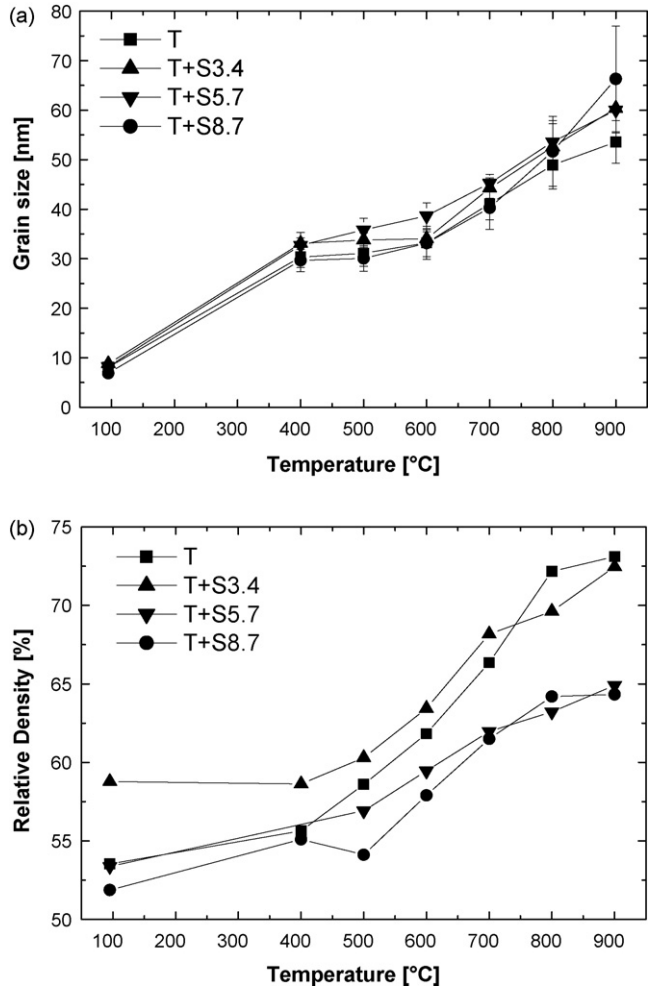


Fig. 1. (a) Grain size vs. sintering temperature for the four specimens T, T + S3.4, T + S5.7 and T + S8.7 and (b) corresponding relative density vs. sintering temperature curves for the above samples.

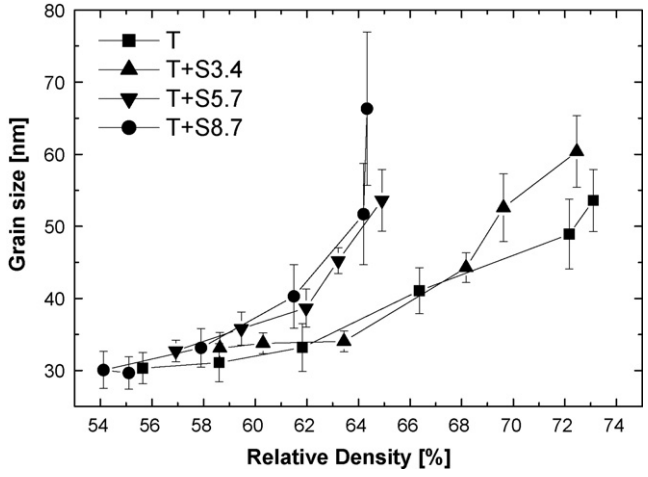


Fig. 2. Sintering trajectories of the specimens T, T + S3.4, T + S5.7 and T + S8.7.

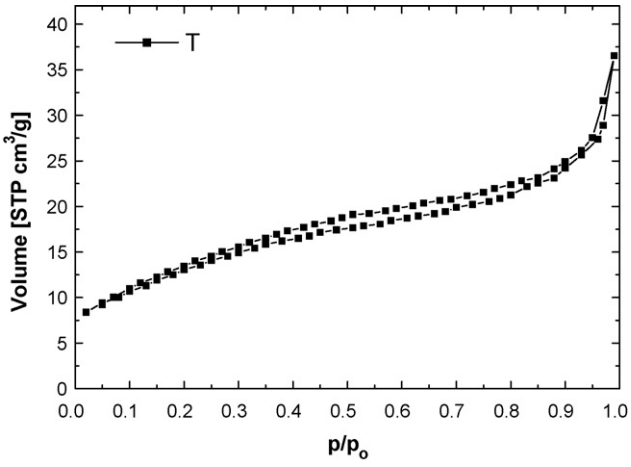


Fig. 3. A typical nitrogen adsorption isotherm of a non-sintered pure titania film.

As nearly all hysteresis loops of the different specimens do not close, the pore size distributions were consistently calculated with the adsorption data as proposed by the IUPAC classification.[22]

Fig. 4 provides the pore size distributions of the pure anatase film T Fig. 4(a) and the film T + S8.7 Fig. 4(b) after sintering at different temperatures. The maxima of the pore size distributions progressively move to larger values as the sintering temperature is increased. For example, the pore size maxima in film T increases from less than 4 nm in the green body to 8 nm and 10 nm after sintering at 700 °C and 900 °C, respectively. Simultaneously, the total amount of adsorbed gas decreases. The films T + S3.4 and T + S5.7 show the same general trends and are therefore not shown here. The pore size distributions of the green films exhibit a bimodal behaviour, exhibiting two maxima at different pore diameters. For sintering temperatures of 700 °C or higher, the pore size distributions convert to a more monomodal character.

The influence of the second phase tin(IV) oxide on the pore size distribution can be assessed using Fig. 5, where comparisons of the pore size distributions of all four films at sintering temperatures of 800 °C Fig. 5(a) and 900 °C Fig. 5(b) are shown. The pore size maxima of the composite films are shifted slightly to higher diameters, compared to the pure $TiO_2$ films, and this is especially true for the material with the highest tin oxide content.

XEDS investigations provide the tin distribution in the T + S8.7 film sintered at 900 °C. Fig. 6 shows an annular dark field (ADF) image of two adjoining anatase grains together with the corresponding elemental maps for oxygen, titanium and tin. The oxygen and the titanium maps clearly highlight the grain boundary between the two grains. The tin map shows a random distribution over the whole area analyzed and does not show any particular enrichment in the grain boundary region. Lower magnification survey views were also taken and confirm that tin is randomly distributed throughout the microstructure and that no separate tin oxide grains were present.

Sn diffusion behaviour in the composite can be further assessed by characterizing the sharpness of the interface between the pre-deposited tin oxide and rutile overlayer (rutile film). This interface, after sintering at 900 °C for 30 min, shows a distinct Sn diffusion gradient into the titania layer in Fig. 7a. Corresponding ADF images and elemental maps of the same $SnO_2$-rutile film structure only sintered at 700 °C (Fig. 7b) suggest that the diffusion of the $SnO_2$ into the $TiO_2$ layer is beginning at 700 °C. A discrete tin oxide layer can still clearly be seen, which is starting to become diffuse. A slight tin gradient into the titania layer is visible. Images of green specimens (not shown here) demonstrate that the tin(IV) oxide layer and the titania layer form a sharp interface without significant diffusion or reaction between the two oxides.

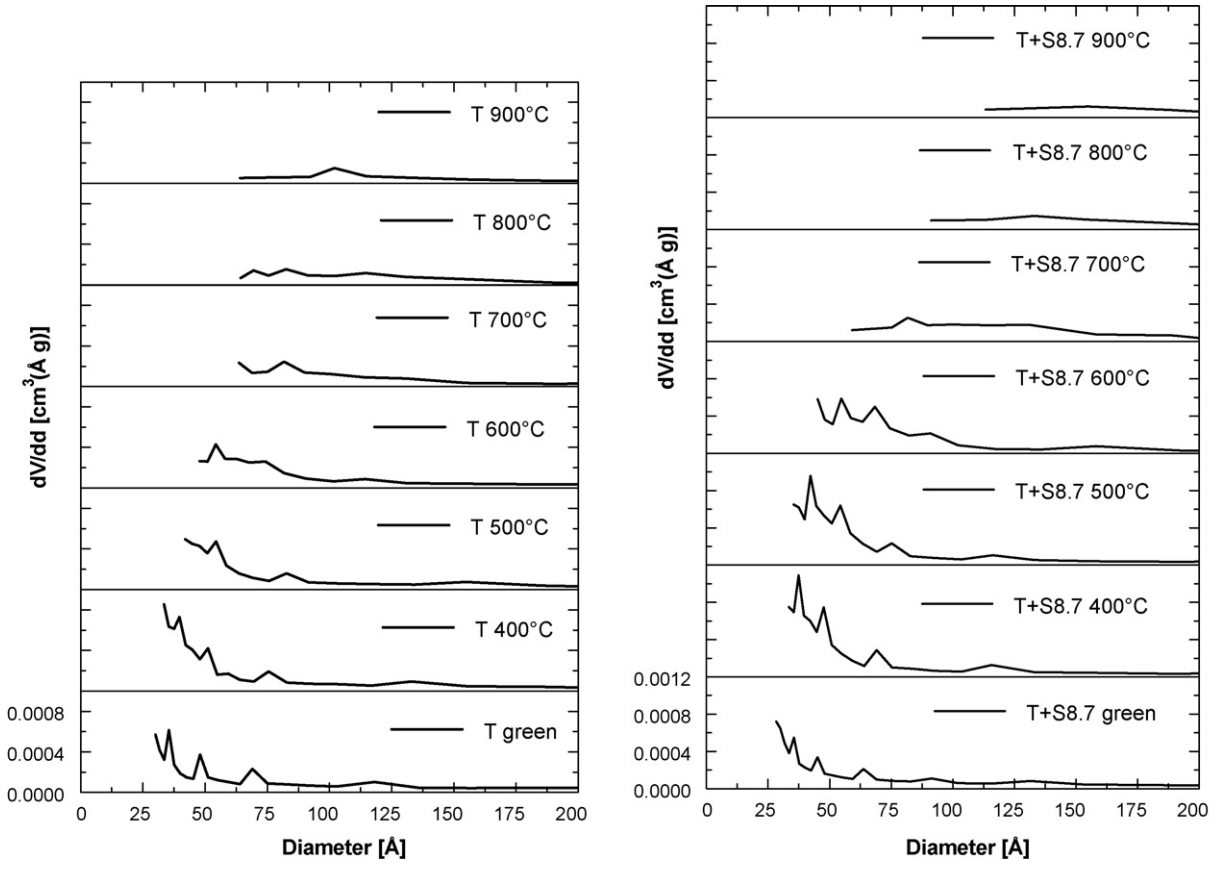


Fig. 4. (a) Pore size distribution of pure titania film T after sintering at different temperatures and (b) pore size distribution of titania film doped with 8.7 wt.% $SnO_2$ after sintering at different temperatures.

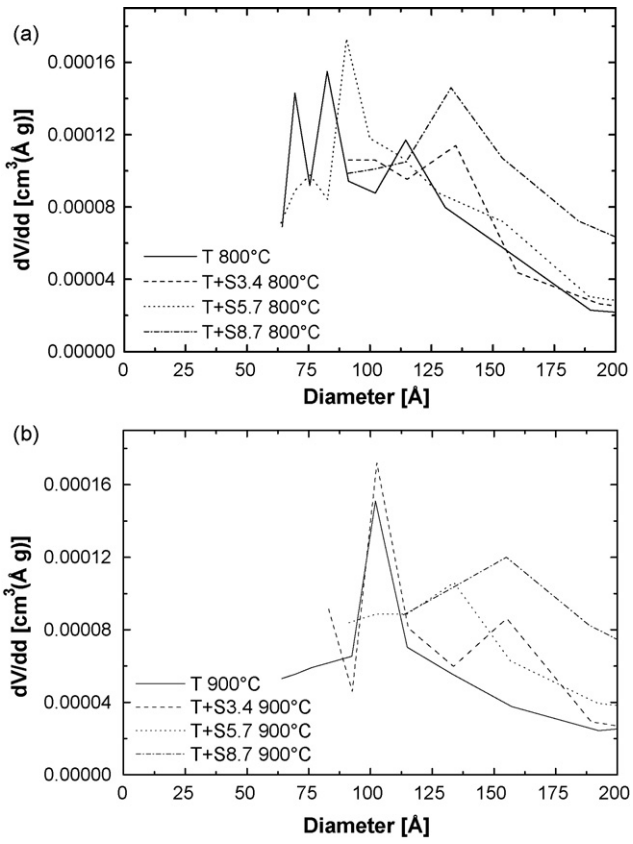


Fig. 5. Pore size distribution of specimens T, T + S3.4, T + S5.7 and T + S8.7 after sintering at (a) 800 °C and (b) 900 °C.

## 4. Discussion

In this study, we encountered four salient issues:

(1) Phase transformation from anatase to rutile as affected by geometrical constraint and tin oxide addition.
(2) Densification of a titania/tin oxide composite as affected by phase transformation.
(3) Grain growth of a titania/tin oxide composite as affected by phase transformation.
(4) Necessary amendments to the phase diagram between tin oxide and titanium oxide.

We will discuss these topics in the sequence provided above.

### *4.1. Phase transformation from anatase to rutile as affected by geometrical constraint and tin oxide addition*

Our results show, that the undoped anatase film and the anatase film containing a small amount of tin oxide do not exhibit a phase transformation to rutile even after sintering at 850 °C. Higher contents in tin oxide lead to a small amount of rutile in the dried film with almost complete conversion to rutile after sintering at 850 °C. The case of the pure anatase film is corroborated by previous literature reports, which state that $TiO_2$ does not transform from anatase to rutile during sintering under constraint[10,11] at temperatures less than 850 °C. Bulk nanocrystalline titania, in contrast, transforms from anatase to rutile at temperatures between 600 °C and 900 °C,[8,9,11] with additions of $SnO_2$ reducing the transformation temperature.[9] Data on thin film sintering of $TiO_2$–$SnO_2$ composites are not available in the literature. These trends can easily be rationalized: as there is a large reduction in molar volume in the transformation from anatase to rutile, the in-plane tensile stress in constrained sintering[26] will oppose the phase transformation, thus leading to an increase in transformation temperature. Additions of tin oxide, in contrast, serve as nuclei for the phase transformation and reduce the transformation temperature.

### *4.2. Densification of a titania/tin oxide composite as affected by phase transformation*

We have succeeded in manufacturing high quality thin films of both pure titania and titania/tin oxide composite. The pore size distributions from the sintered single-phase film are comparable to the pore size distributions of the sintered composite films (see Fig. 4a and b). This is a good indication for a homogeneous distribution of the second phase ($SnO_2$) and a homogenous microstructure.

Comparison of Table 1 and Fig. 2 provides compelling correlation of densification with rutile content in the sintered films.

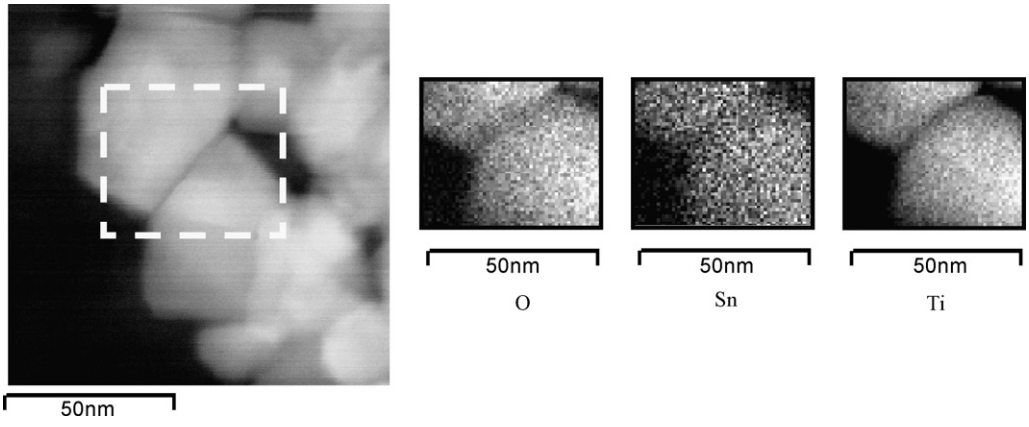


Fig. 6. Annular dark-field image, and O Kα, Ti Kα and Sn Lα XEDS elemental maps of the T + S8.7 film sintered at 900 °C for 30 min.

Thin films, which show no phase transformation from anatase to rutile in the sintered film, densify well, whereas a phase transformation from anatase to rutile is accompanied by poor densification behaviour in the sintered film.

Tensile stresses, which develop during sintering under constraint, hinder the densification of the layer.[26] If there is an additional decrease of volume of about 8%[10] due to the transformation from anatase to rutile, the stresses in the layer increase and the densification is further hindered. Hence, the lower measured relative densities of the titania layers doped with 5.7 wt.% and 8.7 wt.% tin(IV) oxide as compared to the pure anatase film (T) and the 3.5 wt.% $SnO_2$-doped film (T + S3.4) are rationalized.

### *4.3. Grain growth of a titania/tin oxide composite as affected by phase transformation*

The combination of a very fine grain size (8 nm) and very small intra-agglomerate pores (<4 nm in diameter) allows for grain growth (Fig. 1a), with an attendant change of the pore size distribution (Figs. 4a and 5a). These factors are consistent with earlier work on single-phase titania thin films[11] and reflect the strong tendency for agglomeration of nanocrystalline powders.[27]

The pore size distributions in the green films and in the films with limited densification are first bimodal indicating the existence of intra-agglomerate pores as well as inter-agglomerate pores. The maximum of the inter-agglomerate pores increases in dimension due to grain growth and pore coalescence at densities between 60% and 74%, as observed before in thin films of nanocrystalline titania.[11] For sintering at 700 °C or higher, the intra-agglomerate pores have shrunk and only the inter-agglomerate pores remain, yielding a monomodal pore size distribution (Figs. 4 and 5).

In our studies, tin oxide was not suitable as a grain growth inhibitor, since the second phase did not significantly affect the grain growth of the $TiO_2$, which was measured as a function of sintering temperature. If grain growth at comparable densities is considered, then the composites with high content of second phase ($SnO_2$) rather exhibit an increased grain growth rate (Figs. 1a and 2). In detail, the sintering trajectory highlights the strong difference between the single-phase film (film T) and the material with the low tin oxide content (film T + S3.4) on one side and the thin films with the higher tin oxide contents (films T + S5.7 and T + S8.7) on the other side (Fig. 2).

The composite films with high tin oxide content (film T + S5.7 and T + S8.7) contain a high density of rutile grains, which are

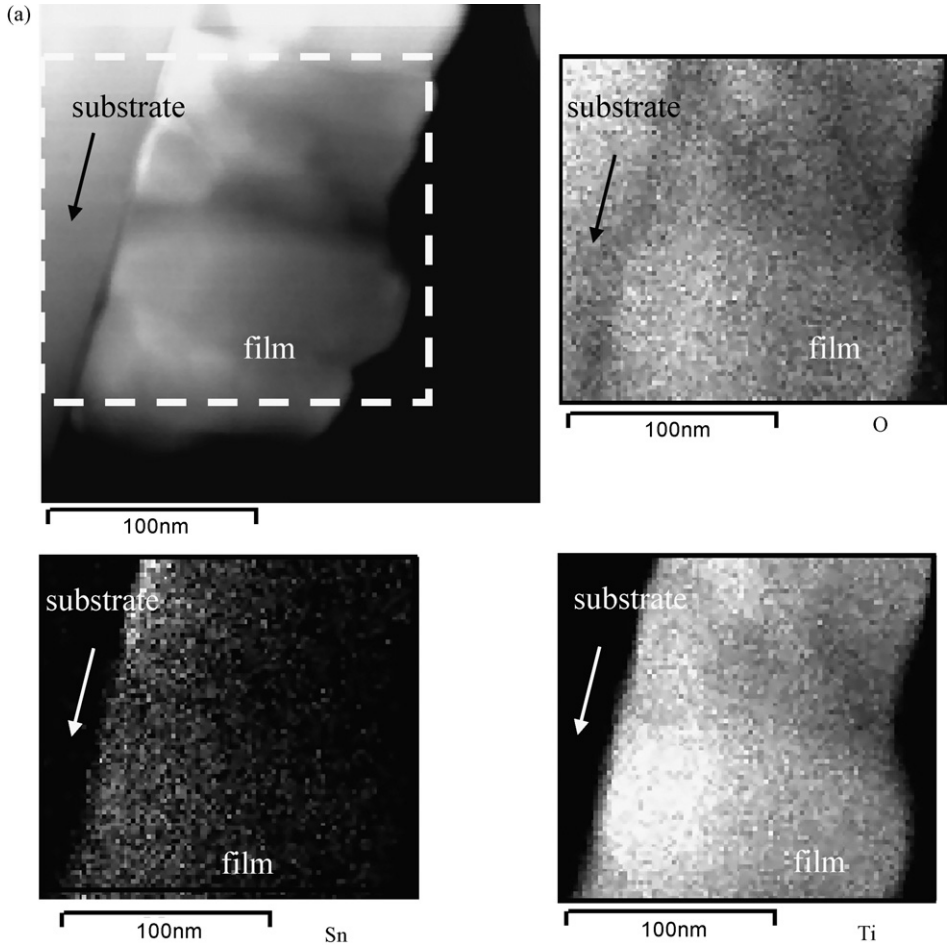


Fig. 7. Annular dark-field image, and O Kα, Ti Kα and Sn Lα XEDS elemental maps of the (a) rutile film sintered at 900 °C for 30 min and (b) rutile film sintered at 700 °C, 30 min.

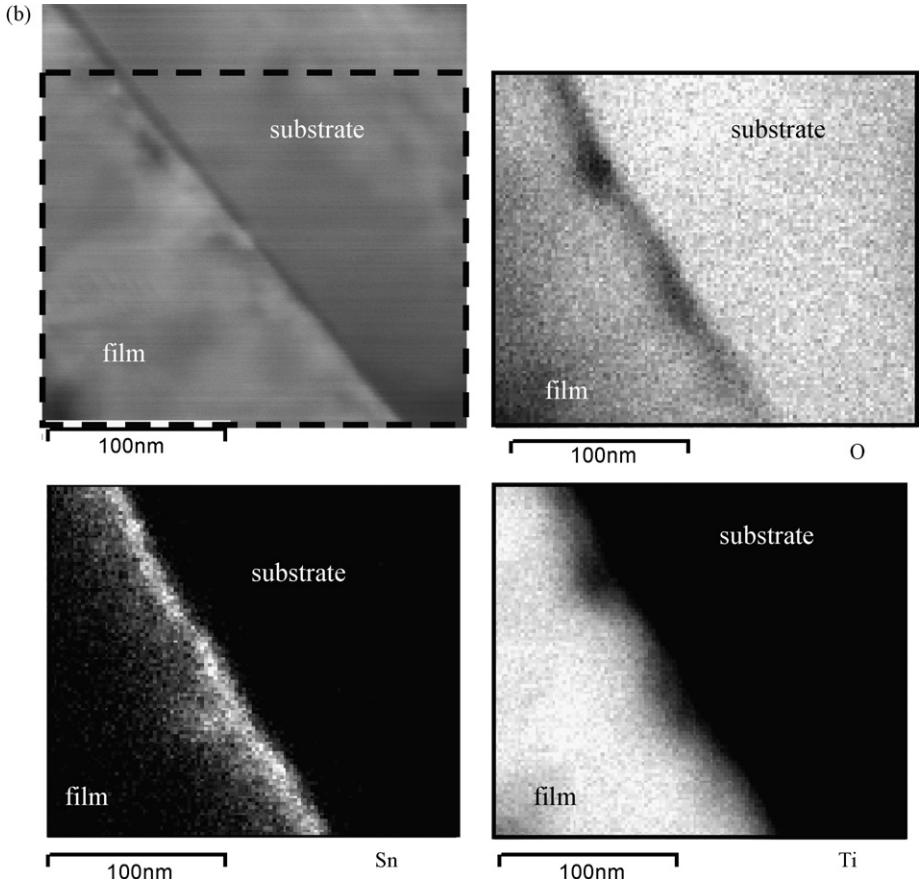


Fig. 7. (*Continued*).

already available to transform anatase to rutile even under constrained conditions. Grain growth of a rutile grain into an anatase grain, therefore is driven both by grain–boundary curvature as well as by the difference in free energy between rutile and anatase. Thus, the increased grain growth during the stage of phase transformation can be rationalized.

### *4.4. Necessary amendments to the phase diagram between tin oxide and titanium oxide*

The examination of the spatial distribution of the Sn was carried out in order to check for the effectiveness of the mechanism of grain growth inhibition through the existence of an inert second phase. Before carrying out STEM studies it was anticipated that separate tin(IV) oxide and the titania grains in the T + S specimens existed concurrently. The publication by Naidu et al.,[17] where the development of the low temperature phase diagram of the $TiO_2$–$SnO_2$ system is described, suggested that below 1000 °C no solid solution should be possible. Only at high temperatures are tin(IV) oxide and titania thought to be miscible, since at lower temperatures a miscibility gap exists.[17] As the diffusion in the solid state is too slow, Naidu et al. used the molten salt method to obtain the low temperature phase diagram and thus determine the extent of the miscibility gap. Hence, our initial expectation was that the diffusion for the creation of a solid solution of $SnO_2$ and $TiO_2$ below 1000 °C is also too slow. In contrast, STEM–XEDS results from the rutile films demonstrate the existence of a solid solution of $SnO_2$ and $TiO_2$ at 900 °C (Fig. 7a). The element maps from the samples sintered at 700 °C (Fig. 7b) show a distinct tin(IV) oxide layer and a small tin gradient extending into the titania layer. The tin(IV) oxide layer therefore actually starts to dissolve into the $TiO_2$ layer when a temperature somewhere slightly below 700 °C. Hence, our high-resolution studies, suggest, that the miscibility gap is at considerably lower temperatures than described by Naidu et al.[17]

The T + S8.7 films sintered at 900 °C showed similar behaviour (Fig. 6). Only a solid solution of $SnO_2$ and $TiO_2$ was found. No separate tin(IV) oxide grains were detected. Investigations of green samples of the T + S8.7 films were not possible since these were not thin enough to resolve individual $SnO_2$ grains. The grains in the green state have a diameter of around 8 nm and therefore for TEM specimens with a thickness of around 40–60 nm we are always projecting through 5–8 grains.

Hence, the development of a solid solution of titania and tin(IV) oxide cannot lead to a grain growth inhibition since there is no second phase which can hinder grain boundary motion. In comparison, Shi et al.[12] observed smaller titania grain sizes with increasing content of tin oxide. This is not inconsistent, as this appears to be not an effect of grain growth, but of smaller initial crystallite sizes in the conversion from the gel to the nanocrystalline material.

## 5. Summary

Homogeneous titania/tin oxide thin films were successfully manufactured. However, tin(IV) oxide was not found to be effective as a grain growth inhibitor. Rather, above a critical level of second phase tin oxide content, rutile grains formed in the green body and provided nuclei for the phase transformation from anatase to rutile during sintering, which is otherwise hindered due to the intrinsic biaxial film stress. This phase transformation is accompanied by significant volume shrinkage and thus leads to a decrease in density in the film. This in turn triggers an increase in biaxial tensile stress in the film, reducing the overall driving force for sintering. An additional driving force for grain growth arises due to the difference in free energy between growing rutile and shrinking anatase grains.

Further, detailed STEM–XEDS investigations proved that tin from nanocrystalline tin oxide grains diffuses into the titania matrix and leads to a homogeneous distribution of tin. This observation was corroborated with the assessment of the diffuse nature of a thin tin oxide layer after it had evolved from a sharp interface during heat treatment at 900 °C.

## Acknowledgment

We would like to thank the Merck KGaA, Darmstadt, Germany, for financial support.

## References

1. Graetzel, M., Photo-electrochemical cells. *Nature*, 2001, **414**(6861), 338–344.
2. Graetzel, M., Nanocrystalline ceramic films for efficient conversion of light into electricity. *J. Sol–Gel Sci. Technol.*, 1994, **2**, 673–677.
3. Berto, A. M., Ceramic tiles: above and beyond traditional applications. *J. Euro. Ceram. Soc.*, 2007, **27**(2/3), 1607–1613.
4. Heller, A., Chemistry and application of photocatalytic oxidation of thin organic films. *Acc. Chem. Res.*, 1995, **28**, 503–508.
5. Paz, Y., Luo, Z., Rabenberg, L. and Heller, A., Photooxidative self-cleaning transparent titanium dioxide films on glass. *J. Mater. Res.*, 1995, **10**(11), 2842–2848.
6. Lee, D., Rubner, M. F. and Cohen, R. E., Al-nanoparticle thin-film coatings. *Nano Lett.*, 2006, **6**(10), 2305–2312.
7. Zhao, J., Wang, L., Wang, L., Yang, H. and Zhao, M., Effect of nuclei on the formation of rutile titania. *J. Mater. Sci. Lett.*, 1998, **17**, 1867–1869.
8. Hague, D. C. and Mayo, M. J., The effect of crystallization and phase transformation on the grain growth of nanocrystalline titania. *Nano Struct. Mater.*, 1993, **3**, 61–67.
9. Kumar, K.-N., Fray, D. J., Nair, J., Mizukami, F. and Okubo, T., Enhanced anatase-to-rutile phase transformations without exaggerated particle growth in nanostructured titania–tin oxide composites. *Scripta Mater.*, 2007, **57**, 771–774.
10. Kim, Y.-J. and Francis, L. F., Microstructure and crystal structure development in porous titania coatings prepared from anhydrous titanium ethoxide solutions. *J. Mater. Sci.*, 1998, **33**, 4423–4433.
11. Stech, M., Reynders, P. and Rödel, J., Constrained film sintering of nanocrystalline $TiO_2$. *J. Am. Ceram. Soc.*, 2000, **83**(8), 1889–1896.
12. Shi, Z. M., Yan, L., Jin, L. N., Lu, X. M. and Zhao, G., The phase transformation behaviours of $Sn^{2+}$-doped titania gels. *J. Non-Cryst. Solid*, 2007, **353**, 2171–2178.
13. Hahn, H., Logas, J. and Averback, R. S., Sintering characteristics of nanocrystalline $TiO_2$. *J. Mater. Res.*, 1990, **5**(3), 609–614.
14. Chen, P.-L., Chen, I.-W. and Chen, Sintering of fine oxide powders. 2. Sintering mechanisms. *J. Am. Ceram. Soc.*, 1997, **80**(3), 637–645.
15. Kanters, J., Eisele, U. and Rödel, J., Effect of initial grain size on sintering trajectories. *Acta Mater.*, 2000, **48**, 1239–1246.
16. Srdic, V. V., Winterer, M. and Hahn, H., Sintering behaviour of nanocrystalline zirconia doped with alumina prepared by chemical vapour synthesis. *J. Am. Ceram. Soc.*, 2000, **83**(8), 1853–1860.
17. Naidu, H. P. and Virkar, A. V., Low-temperature $TiO_2$–$SnO_2$ phase diagram using the molten-salt method. *J. Am. Ceram. Soc.*, 1998, **81**(8), 2176–2189.
18. Iida, Y., Furukawa, M., Aoki, T. and Sakai, T., Raman spectroscopy of ultrafine anatase powders derived from hydrolysis of alkoxide. *Appl. Spectrosc.*, 1998, **52**(5), 673.
19. Ambrosius, K., Esselborn, H., Knapp, A., Plamper, H. and Esselborn, R., Verfahren zur Herstellung von mit Rutil beschichteten Glimmerpigmenten. Pearl pigment production—by successive deposition of tin oxide and titanium dioxide on mica flakes contg. aq. suspension. Merck Patent GMBH EP 0271767 B1; DE 364,647; US 4,867,794, December 13, 1986.
20. Brunauer, S., Emmett, P. H. and Teller, E., Adsorption of gases in multimolecular layers. *J. Am. Ceram. Soc.*, 1938, **60**, 309–319.
21. DIN66 131, *Bestimmung der spezifischen Oberfläche von Feststoffen durch Gasadsorption nach Brunauer*. Emmett und Teller (BET), 1993.
22. International Union of Pure and Applied Chemistry (IUPAC), Sing, K. S., Everett, D. H., Haul, R. A. W., Moscou, L., Pierotti, R. A., Rouquerol, J. and Siemieniewska, T., Reporting physisorption data for gas/solid systems with special reference to the determination of surface area and porosity. *Pure Appl. Chem.*, 1985, **57**(4), 603–619.
23. DIN 66134, *Bestimmung der Porengrößenverteilung und der spezifischen Oberfläche mesoporöser Feststoffe durch Stickstoffsorption*, 1998.
24. ASTM D 4641–94, *Standard practice for calculation of pore size distribution of catalysts from nitrogen desorption isotherms*. März, 1994.
25. Barrett, E. P., Joyner, R. and Halenda, P. P., The determination of pore volume and surface area distribution in porous substances. I. Computations from nitrogen isotherms. *J. Am. Ceram. Soc.*, 1951, **73**, 373–380.
26. Green, D. J., Guillon, O. and Rödel, J., Constrained sintering: a delicate balance of scales. *J. Eur. Ceram. Soc.*, 2008, **28**(7), 1451–1466.
27. Kounga Nijwa, A. B., Aulbach, E., Rödel, J. and Neubrand, A., Mechanical properties of dry-pressed powder compacts: case study on alumina nanoparticles. *J. Am. Ceram. Soc.*, 2006, **89**(8), 2614–2644.